JOURNAL OF AIRCRAFT
Vol. 44, No. 2, March–April 2007

Computational Analysis of Wake Vortices Generated by Notched Wings

Z. Zouaoui,* L. Szkatula,† and R. J. Grant‡
NEWI-University of Wales, Wrexham, LL11 2AW, United Kingdom

DOI: 10.2514/1.23918

The motivation behind the present investigations is the alleviation of vortex wake hazard. The present paper contains a 3-D computational analysis of the trailing wake vortices generated by notched (rectangular) wings, at a chord-based Reynolds number of 5.34×10^4. Various wing configurations were tested to determine the quantitative and qualitative effects of wing geometries on vortex dynamics. Two sets of computations were conducted up to 80 chord lengths downstream from the tip region. The first set used the conventional and notched-wing geometries for correlation of experimental and computed results. The second set of simulations concentrated on the development and testing of new wing designs. Wing geometries combined multiple tip (triangular/ogee) forms with the original notch design. The nature of vortices was classified in terms of their location, strength, and trajectories. Flow data were analyzed within these categories, at different crossflow planes behind the trailing edge. The first set of computational solutions demonstrated that the notched geometry significantly influenced the vortex location and strength of the wake system. The numerical results also confirmed that the tip and flap vortices generated by a notched wing remain distinct and unmerged, unlike those associated with the conventional wing. Finally, computed data demonstrated that the two-equation renormalization group k–ϵ turbulence model, combined with an appropriate treatment of the near-wall region is capable of predicting accurately steady and turbulent flows past wings. Very good agreement was obtained between the experimental and numerical results. Numerical simulations were performed for the second set of wing geometries to evaluate the effectiveness of wing modifications on the wake properties. Current results are promising: for all the cases considered, the wakes of the notched-triangular/ogee wings show maximum vorticity magnitudes that are substantially lower than those generated by the original notched wing. Numerical data clearly indicate that such geometrical combinations significantly reduce the wake strength and affect the merging process of the present vortex system.

Nomenclature

b_{TF}	=	tip-flap vortex separation distance
c	=	wing chord
dA	=	cross section area
k	=	turbulent kinetic energy
r	=	radial distance
r_c	=	vortex core radius
Re	=	chord-based Reynolds number
s	=	wing semispan
U	=	upstream velocity
u, v, w	=	flow velocities in x, y, z directions
v_θ	=	tangential velocity
x, y, z	=	Cartesian coordinate system
Γ	=	vortex strength
ϵ	=	dissipation rate of turbulent kinetic energy
ω	=	streamwise vorticity

I. Introduction

THE Federal Aviation Administration (FAA) predicted that by the year 2010, over a billion passengers a year will be traveling by air [1]. To keep the number of new airports and runways to a minimum, there is an urgent need to increase their efficiency without compromising safety. It is well known that wake vortices generated by aircraft are a danger for any following aircraft that fly through them [2,3]. Rolling motion, structural loads, and loss of control, possibly leading to ground impact, may occur during an encounter with a wake. As a result, minimum separation distances for landing aircraft were imposed by the International Civil Aviation Organization (ICAO) and the FAA in the 1970s and those have remained essentially unchanged to this day. Although separations standards have proven to be effective from a safety point of view, they are empirical and frequently well in excess of the spacing required. They significantly reduce airport operational capacities, impose costly delays, and incur large fuel losses [4]. The aircraft industry is currently developing larger aircraft with capacity as high as 840 passengers. The question of suitable separations for the new super-Jumbo, namely, the Airbus A-380, remains open. It is believed that the present regulations will simply not be adequate to meet the demand. A quantitative measure of the penalties imposed by wake vortex separation distances can be obtained by considering a simulation of a runway operating with a 3 n mile IFR radar spacing and a full capacity of 30 operations per hour. If the separation between aircraft using the runway is increased to 5 n miles, the capacity would be cut by a third, i.e., 20 operations per hour, and in turn a 7 n mile separation would give a capacity of 15 operations per hour. Different ways have been explored to decrease the spacing standard between aircraft [5–7]. However, only one strategy is used in the present research work: any wing modifications, including end-tip and end-flap, which will reduce wake vortex intensity and/or accelerate the vortex decay are highly desirable.

Growth in the aviation industry is currently being driven by efforts to reduce costs through improved processes rather than by new technology. This has led to some evolutionary, rather than revolutionary technology. As a result it could be considered timely to investigate new designs and unconventional concepts, such as the notch design or any other advanced wing designs involving triangular or ogee concepts. In recent research work [7,8], it was

Presented as Paper 245 at the 44th AIAA Aerospace Sciences Meeting and Exhibit, Reno, NV, 9–12 January 2006; received 15 March 2006; revision received 14 June 2006; accepted for publication 7 August 2006.

*Reader, Department of Aeronautical Engineering; z.zouaoui@newi.ac.uk.

†Ph.D. Candidate, Department of Aeronautical Engineering; l.szkatula@newi.ac.uk. Member AIAA.

‡Principal Lecturer, Department of Aeronautical Engineering; r.j.grant@newi.ac.uk.

stated that it is possible to significantly reduce wake vortices by optimizing the wing lift distribution via the wing shape. In fact, experiments [9] conducted in a towing tank at Cambridge University demonstrated that the notch configuration creates a drop in the wing lift distribution, generating a region of counter-rotating vorticity, referred as the negative region, located between the tip and the flap vortices, which is seen to prevent the merging of the tip and flap vortices far downstream the trailing edge. It has been observed that long-term separation of the tip and flap vortices has the potential to reduce wake vortex strength. Another potential way of reducing wake hazard includes eliminating or minimizing geometrical irregularities, such as 90 deg corners. It was noticed that inboard and outboard flaps, in addition to rectangular end-tips, strongly affect flow features, especially in landing and takeoff configurations. Combinations of the notched design with new concepts, such as the novel triangular and ogee profiles proposed in this paper, have proven to greatly affect the wake hazard and reduce the severity of wake vortex phenomenon.

The primary purpose of CFD is to provide new information and tools for the analysis and design of new concepts to meet required performance goals. Such numerical tools can be used at reduced cost, time and risk. Unconventional configurations lying outside the experience base of the designer can then be explored more quickly. However, there is a need to evaluate and assess the validity of the models. This is why it is of fundamental importance, before testing any novel wing geometries, to compare numerical results with experimental data to produce results with sufficient accuracy.

The structure of the paper is as follows. First, Sec. II briefly describes the computational procedure and the geometrical characteristics of the novel wing designs. Experimental and numerical data are compared in Sec. III; CFD parameters are then validated. Numerical results involving new wing designs are presented and analyzed in Sec. IV. Finally, concluding remarks are summarized in Section V.

II. Computational Procedure

A. Wing Geometries

For the present research work, three-dimensional models of half rectangular wings were developed. Two separate data sets were considered: the first set (set 1) included the exact geometries used in [9] to reproduce experimental results, whereas the second set (set 2) investigated the wake properties of notched-triangular/ogee wings. The first set of computations was performed using two different wing models: the conventional and the notched wing referred to as models 1 and 2 (Fig. 1). For both models the environment and conditions found in experimental towing tank are recreated numerically. Both wings have a rectangular planform with a cambered plate geometry cross section. The mean chord c is 100 mm and the semispan s is 300 mm. The cross section camber is circular with a radius of curvature of 210 mm, thickness of 2 mm, and a nose radius of 1 mm. The trailing edge remains straight: perpendicular to the top and the bottom surfaces. For the conventional wing, the inboard flap (16×183 mm) is extended by 20 deg. Model 2 uses a combination of a rectangular platform and a notch; the root chord is 105 mm long whereas the tip chord is 102 mm. Inboard (15×135 mm) and aileron flaps (12×75 mm) are extended by 20 deg as well. Using the previous cross section and geometries as a starting point, a number of different geometrical changes were generated and analyzed numerically for set 2. The notch design remained unchanged (notch depth, width, and location were kept as original) and only the end-tip shapes were varied. Triangular and ogee end-tips were both considered at various locations. Alterations in cut cross section were achieved with respect to the distance along the chord (7, 50, and 60%) and along the span (75, 80, and 87%). A specific classification was created, which included the chord position, the section used (triangular or ogee), and the location along the span, respectively. In turn, models 3–9 are referred to as N7Tri75, N7Sik75, N50Tri75, N50Sik75, N50Sik80, N50Sik87, and N60Sik87. A variety of wing shapes could have been tested using either triangular or ogee concepts for the end-tips, with or without the notched configuration, along with the modification of the flap extension. From a large number of trials, set 2 wing geometries constituted a panel of the best configurations in wake hazard alleviation. Set 2a (Models 3 and 4, Fig. 2) and set 2b (Models 5–9, Fig. 3) included seven variant geometries all coupled with the original notch design. Triangular and ogee sections were selected for various reasons. Testing of triangular shapes has confirmed that they significantly reduce wake vortices and offer significant improvements over current designs [10]. Ogee configurations are well known in biological wings and are shaped by means of a concave arc flowing into a convex arc forming an S-shape curve. Although not many publications are devoted to Sikorsky's investigations of wing design, it was found that such a curved tip can reduce the maximum tangential velocity in the wake vortex to about 25% of that in the wake formed by a normal square tip [11]. In addition, data analyses showed that ogee tips significantly reduce the strengths of the vortices while providing improved flight performance in terms of induced drag [12]. The objective was, therefore, to analyze how the wake flow and the wake topology would be influenced by combining notch and end-tip geometries.

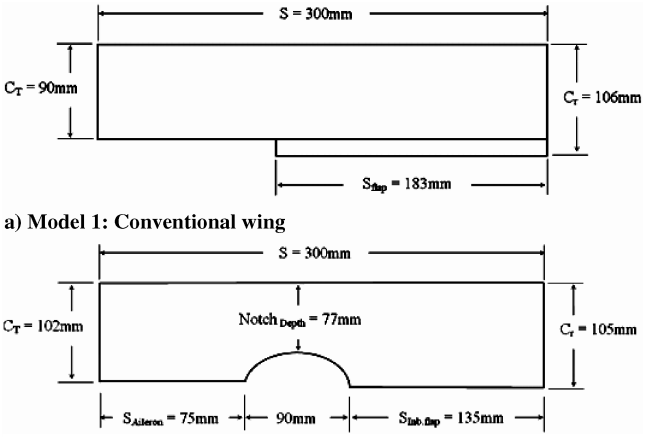

a) Model 1: Conventional wing

b) Model 2: Notched wing

Fig. 1 Wing geometry definition: set 1.

B. Grid Generation

For the present analysis, a regular and structured grid of approximately 3.5×10^6 hexahedral cells (C-H body-fitted grid system) is used to represent the far-field boundaries. Figure 4 shows a close-up view of the grid system used in the present work. Nodes are currently clustered in the chordwise direction near the leading and the trailing edges and in the spanwise direction near the wing tip to provide improved resolution of the wing vortex system. The minimum spacing normal to the wall is 1.0×10^{-5}, and the far-field

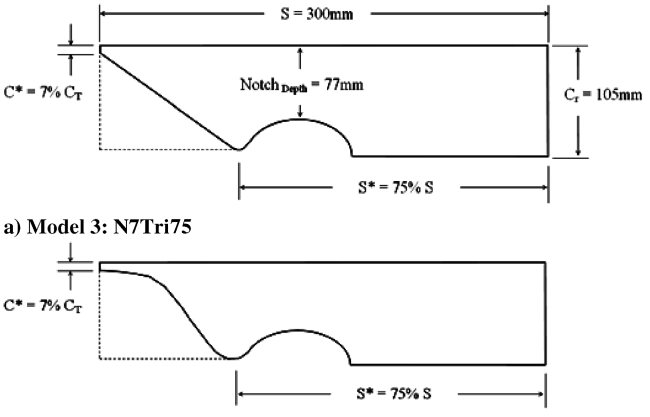

a) Model 3: N7Tri75

b) Model 4: N7Sik75

Fig. 2 Wing geometry definition: set 2a.

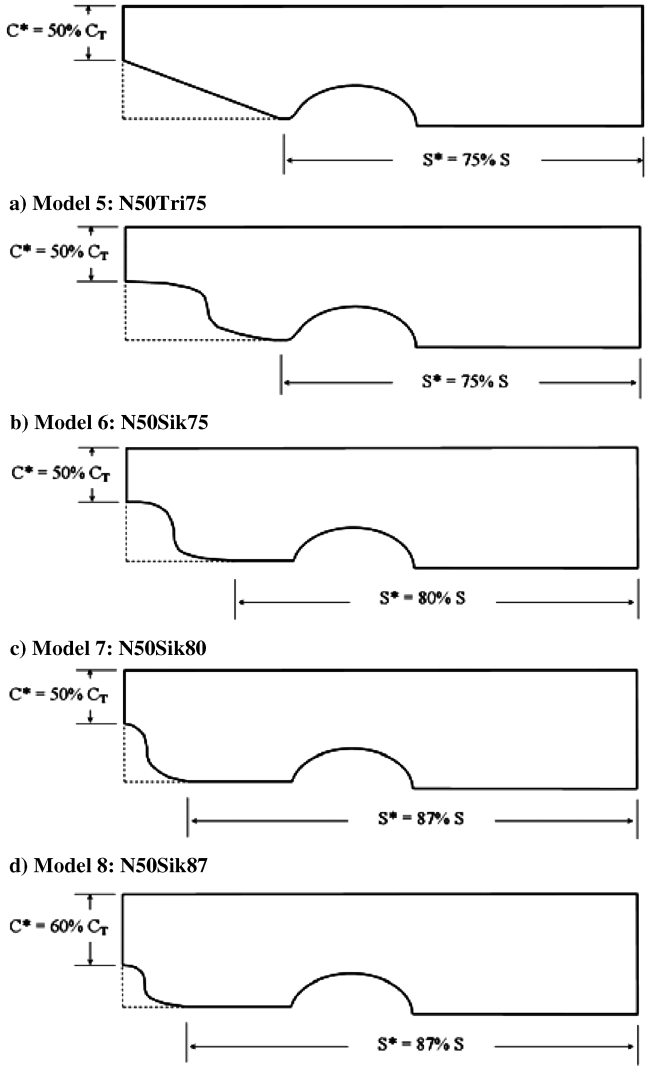

Fig. 3 Wing geometry definition: set 2b.

boundary is located seven root chord lengths away from the tip of the wing. The outflow boundary is located 80 root chord lengths downstream from the trailing edge. To reduce wall interference, the boundaries are kept sufficiently far from the models. The domain of the whole grid is decomposed into three subdomains: the wing surface, the upper side of the wake, and the lower side of the wake. Particular attention is paid to the mesh quality. The resolution of the grid inside the domain is checked by plotting the Y plus (y^+) distribution [13,14] on the wing surfaces. Wall adjacent cells are considered to be in the viscous sublayer ($y^+ \sim 1$).

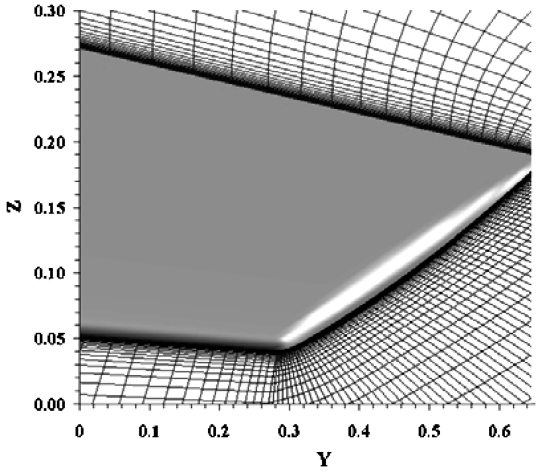

Fig. 4 Details of the regular structured grid close to the wing tip surfaces.

C. Simulations and Flow Parameters

The computational simulations were performed using version 6.2 of the finite-volume based code FLUENT©. Parallel implementation was completed by means of sharing the computation load for each subdomain to each processor element (PE). The numerical model in the present analysis solves the full set of Reynolds-averaged Navier–Stokes equations for a three-dimensional incompressible fluid and a steady-state environment. Turbulence was incorporated using the renormalization group theory (RNG) k–ϵ turbulence model, which demonstrates a good overall convergence and robustness. Although the results are not presented in this paper, flow simulations were performed with laminar and Spalart–Allmaras turbulence models. Because it was observed that the numerical results using the RNG k–ϵ were in better agreement with the experiments and predicted more accurately the locations of the vortices, the former turbulence model was employed. It should be noted that, whereas the k–ϵ model is a high Reynolds number model, the RNG theory provides an analytically derived differential formula for effective viscosity that accounts for low Reynolds number effects [14,15]. Effective use of this feature does, however, depend on an appropriate treatment of the near-wall region. The near-wall modeling significantly impacts on the fidelity of numerical solutions, inasmuch as walls are the main source of vorticity and turbulence. Therefore, accurate representations of the flow in the near-wall region determine successful predictions of the flow characteristics. In the present work, the enhanced wall treatment was employed, enabling the viscosity-affected region to be resolved with a mesh all the way to the wall, including the viscous sublayer. The velocity magnitude at the inlet was 0.534 m/s (chord-based Reynolds number of 5.34×10^4). The angle of attack was set to 0 deg. The flow was modeled as a single component fluid with the properties of water. Convergence to a steady state was generally achieved within approximately 3000 grid cycles, requiring 100–150 CPU hours, depending on the order scheme settings. Solutions are considered converged when the continuity reaches the minimum value of 1.0×10^{-7} and when the change in vorticity magnitude over the last 100 cycles is less than 1.0×10^{-4}.

III. Comparison Between Experimental and Numerical Results: Set 1

The motivation behind these investigations is the validation of the CFD parameters. Experimental data from [9] are compared with predictions obtained from CFD computations, in the form of vorticity fields, circulation, and trajectories.

A. Data Collection and Flow Visualization

Graham et al. [9] present the velocity vectors and corresponding contours of dimensionless vorticity $\omega s/U$ for the conventional and the notched wings at two different measurement planes, located at 1.2 and 39.7 semispans (4 and 132 chord lengths, i.e., $4c$ and $132c$) downstream from the trailing edge, respectively. Computational results are obtained by means of 44 measurement planes with a spacing of $2c$ and compared with the experimental results. The first measurement plane is located at $1c$ downstream from the trailing edge and the last one at $80c$. Because of computer constraints, the maximum computed distance behind the trailing edge is limited to $80c$. Computed data at measurement plane $132c$ are not available and no comparisons are made between experimental and numerical results at this plane. However, additional experimental data are available at $21c$. The measuring planes are normal to the freestream velocity and approximately 1640 data points are taken for each crossflow plane. Vortex cores are localized and the quantities

associated with vortices for each model are derived. Lift distributions are additionally compared.

B. Spanwise Lift Distribution

Significant reductions in vortex strength can be achieved by optimizing the wing lift distribution. By varying the span-loading, the lift distribution is seen to greatly influence the birth, roll-up, and growing of vortex systems [8,9]. Experimental and numerical lift distributions are now compared for the conventional and the notched wings. A map mesh is created on the surface of each wing section and data from each cross section are then integrated. Figure 5 shows the experimental and computed wing lift distributions along the normalized spanwise coordinates (y/s). The lift distribution given by model 1 is that of the conventional wing, whereas the optimum lift distribution corresponds to the notched wing (model 2). As expected, a significant drop in lift distribution, at the notch location, is obtained for model 2. Numerical and experimental lift values given at notch location ($y/s = 0.62$) are in excellent agreement. The computed notched and conventional wing distributions closely match the experimental lift distributions identified by Graham et al. [8,9].

C. Vortex Dynamics: Calculation Methods

The physical vortex properties, such as vorticity, circulation, and centroid locations are discretized on a Cartesian staggered grid and integrated in space and time by second-order finite differencing. Dimensionless vorticity, $\omega s/U$, and circulation values are computed and compared with experimental results for the conventional and the notched wings at various measurement planes behind wing models. Data sets are presented in both normalized and dimensional forms to convey practical information about magnitudes and averaged values. Such analyses produce a vast quantity of results, even for a single-wing model, and only the most relevant data are presented here. The calculation methods are now given. The x-component of vorticity ω_x is calculated using velocity gradients fields:

$$\omega_x = \frac{\partial w}{\partial y} - \frac{\partial v}{\partial z} \tag{1}$$

Vortex strength in the wake and vortex centroids are determined by means of the standard definitions. The wake circulation is obtained by integrating the axial vorticity over the cross section area:

$$\Gamma = \int \omega_x \, \mathrm{d}A \tag{2}$$

and the position $(\bar{y}, \bar{z})$ of the overall vorticity centroid is given by

$$(\bar{y}, \bar{z}) = \frac{1}{\Gamma} \int (y, z) \omega_x \, \mathrm{d}A \tag{3}$$

The tangential velocity V_θ and radial coordinate r are determined from the in-plane velocity components (v, w) and (y, z) coordinates relative to the vortex centroid, respectively. This allows direct determination of the peak tangential velocity and the corresponding radius r_c.

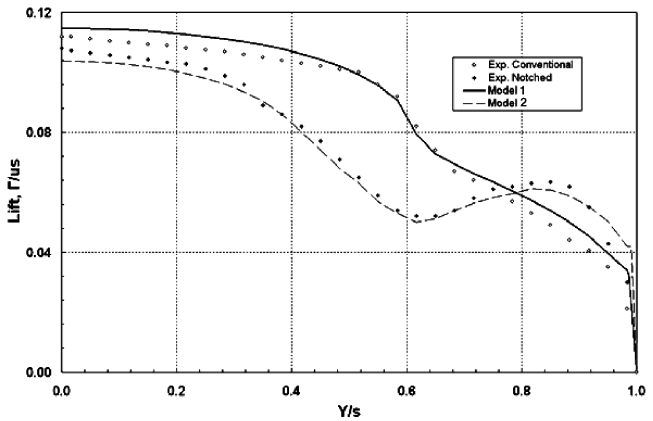

Fig. 5 Experimental and numerical wing lift distributions for the conventional and notched wings.

D. Vortex Contours and Trajectories

Figures 6–8 show the computed and experimental vorticity contour levels for Models 1 and 2 at measurement planes $4c$, $21c$, $80c$, and $132c$. Two and three distinct regions of vorticity are initially created for Models 1 and 2, respectively. Simulations show that the conventional wing creates two vortices with positive swirling from the outside tip and flap (Fig. 6). In comparison, the wing fitted with the notch creates three vortices: two with positive vorticity from the tip and the flap and one with negative vorticity (counter-rotating circulation compared to the corotating vortices produced by the tip and the flap) from the notch (Fig. 6). Tip vortices are located on the right-hand side, whereas flap vortices are located on the left hand side. Figures 6–8 clearly indicate that shapes and positions of vortex cores change gradually in time: core sizes are larger at measurement planes $21c$, $80c$, and $132c$ than at $4c$. This observation is well known and constitutes the diffusive-convective stage of the merging process. Figure 8 displays the computed core positions at $80c$ and the experimental core locations at $132c$, highlighting the location that the computed vortex cores should reach at $132c$. The vortex core growth rate for Models 1 and 2 is illustrated here and it can be seen how the notched geometry modifies the flow in a fundamentally different manner from the conventional wing. The tip and the flap vortices generated by the conventional wing draw closer, and eventually merge forming a unique vortex system (Fig. 8), whereas two distinct vortices, having a well-defined center, are still clearly visible at measurement plane $80c$ and $132c$ for the notched geometry. The tip and the flap vortices for the notched design remain distinct, as expected (Figs. 8 and 10).

Although experimental vortex separation distances are not available, it is believed that showing the computed vortex spacing b_{TF}, for Models 1 and 2, would provide a better understanding of the evolution and merging processes. The vortex spacing b_{TF} is defined as the distance between the tip and the flap vortices, as shown in Fig. 9. The influence of wing geometry on spacing b_{TF} is discussed here. At $54c$ downstream the conventional wing, vortices are subject to a rapid growth in size, which results into the merging of the two vortex systems. An increase of 24% in spacing b_{TF} is achieved for model 2 at $80c$. The dynamics of corotating vortices can be defined into three principal stages, namely, the diffusive and convective stages, followed ultimately by the diffusion of the merged vortex [16]. These stages are best defined with reference to the plot of vortex separation, shown in Fig. 10. The first stage, the diffusive stage, is defined in the present work at interval $X/s = X_A$. Once the vortices are created, they begin to orbit in a cyclonic way around their common center of rotation as shown by the sequence of snapshots in Figs. 6–8. At this stage, vortices are approximately axisymmetric and spacing b_{TF} remains essentially constant. The convective stage is seen at interval $X/s = X_B$: at this stage, vortices grow in radius while rapidly orbiting and drawing towards each other. They become noticeably deformed, adopting essentially an elliptical shape. The vortex centers are pushed together, causing a rapid linear reduction in vortex separation (as seen in Fig. 10, over the distance interval labeled as X_B). Vortices are defined as fully merged when the vortex separation b_{TF} reaches zero. Visualization of the merger process reveals the formation of long filaments at the outer edges of the vortices. Finally, the last phase of the merger mechanism, also called the merged diffusive stage, is initiated at $X/s = X_C$. At this point, the two vortices rapidly merge into a single circular structure, leaving a thin filament spiraling around the merged vortex. The resulting vortex then grows in size and gradually becomes axisymmetric. The evolution of the vortex separation b_{TF} for the notched wing seems to diverge from the evolution observed for the conventional wing. Two main stages are observed, namely, the first and second diffusive stages. The first diffusive period, which is similar to the first stage of the conventional wing, is included in interval $X/s = [0, 4]$. The second diffusive stage replaces the well-known convective stage. In

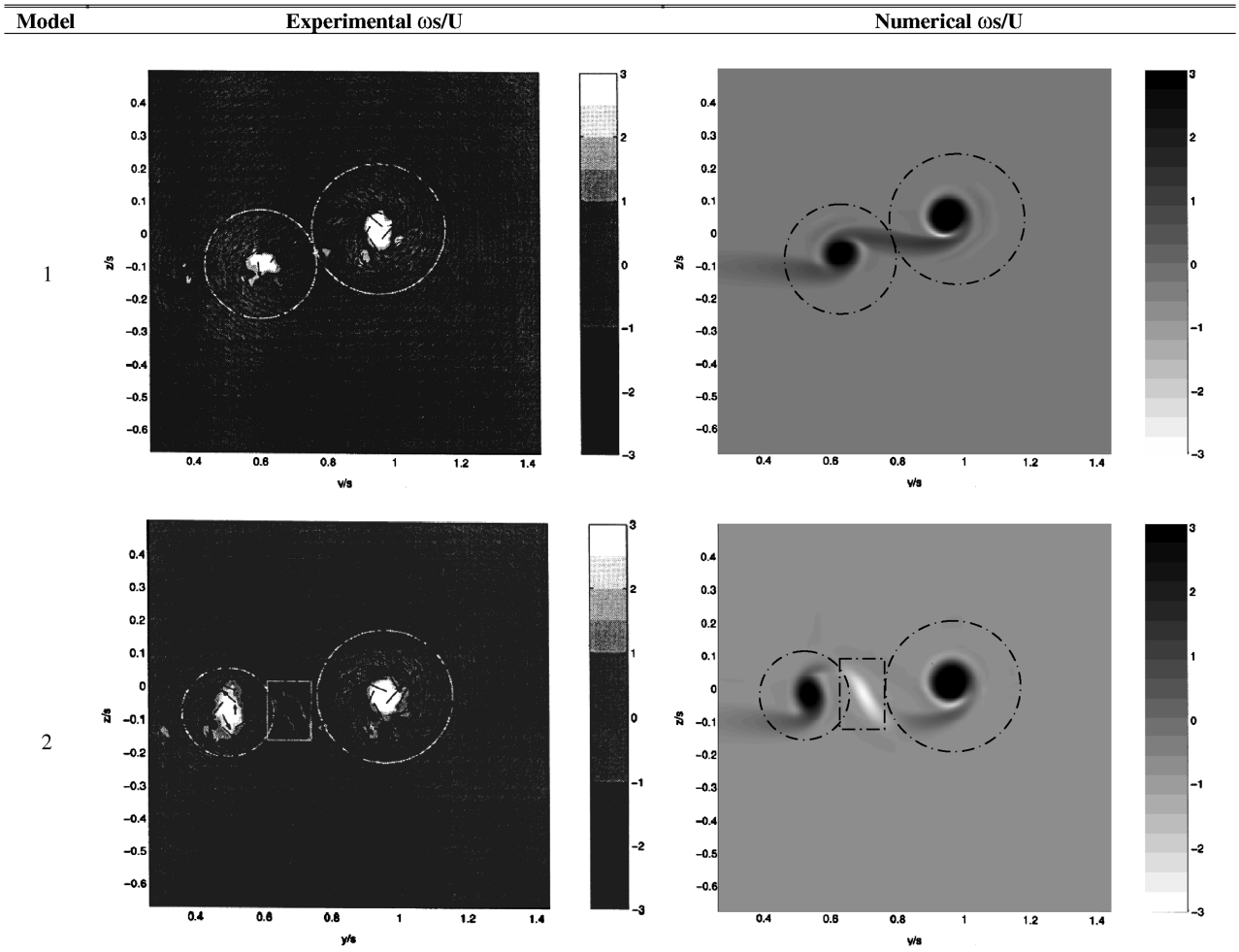

Fig. 6 Vorticity contour levels for models 1 and 2 at 4*c*. Circles indicate the integrated areas for the tip and flap vortex circulation, whereas the rectangle indicates the integrated area for the negative circulation region.

fact, in the case of model 2, the convective period does not exist for the notched wing; the vortices do not stop rotating around one another while the vortex separation constantly increases (at least up to measurement plane 80*c*).

Wake vortex systems trajectories are presented in Figs. 11 and 12. Figure 11 shows the path trajectory followed by wake vortices for the conventional model, whereas Fig. 12 presents the wake trajectories for the notched wing. With regard to model 1, the tip vortex clearly moves downstream upwards while the flap vortex moves downwards. As explained earlier, this phase represents the roll-up process, which preceded the merging. Figure 11 clearly illustrates that the tip and flap vortices for model 1 slowly approach one another and eventually merge. Tip and flap vortex trajectories for model 2 clearly remain distinct, confirming the predictions of [8,9]. The tip vortex converges slightly to the top left while the flap vortex moves downwards and to the right hand side, clearly approaching experimental vortex locations at 132*c*, reproduced in Fig. 8. Therefore, this suggests that experimental and computed vortex contours compare well. It also supports the hypothesis that the aileron extension associated with the flap deflection modifies the vortex dynamics, by causing a divergence between the tip and the flap vortices.

Finally, locations of vortex centroids are analyzed. Data from Tables 1 and 2 demonstrate that vortex centroid locations for the conventional and the notched wings are in excellent agreement with the experimental values. The error between computed and experimental data is less than 5%. Computed plots at the three planes (4*c*, 21*c*, and 80*c*) visually confirm that the locations of vortex cores are close to vortex contours obtained from experimental flow visualization. Comparisons also show that both experimental and numerical trajectories compare very well and converge to a similar path.

E. Vorticity Fields and Circulation

The main interest lies in the vorticity and circulation fields, which hold the crucial information and determine the characteristics of the wake. Tables 3 and 4 list discrepancies in vorticity core magnitude between computed and experimental data, for the conventional and the notched wings at various measurement planes. Experimental vorticity values for Models 1 and 2, at 4*c*, are approximately equal to 3 excluding any magnitude differences between the tip and the flap vortex. Numerical results reveal that vorticity values at the core center for Models 1 and 2 are increased by coefficients up to 5 compared to experimental data. Furthermore, tip and flap vortices present different levels of vorticity magnitude. Such discrepancies at core center are likely to be attributed to the fact that digital particle image velocimetry (DPIV) is used to determine vortex quantities. Experimental vorticity values at core center are prone to large errors due to the fact that it is practically impossible to determine with an extreme precision the location of the center core and its associated vorticity magnitude, compared to CFD simulations. On the other hand, the computed vortex quantities given at core center are extremely localized and represent the maximum value for a unique central core cell. The surrounding area of this single cell is exposed to different vorticity levels (see Figs. 6–8 for the dimensionless vorticity contours). In this case, the tip and the flap vorticity magnitudes for Models 1 and 2, at surrounding cells are equal to 4.5

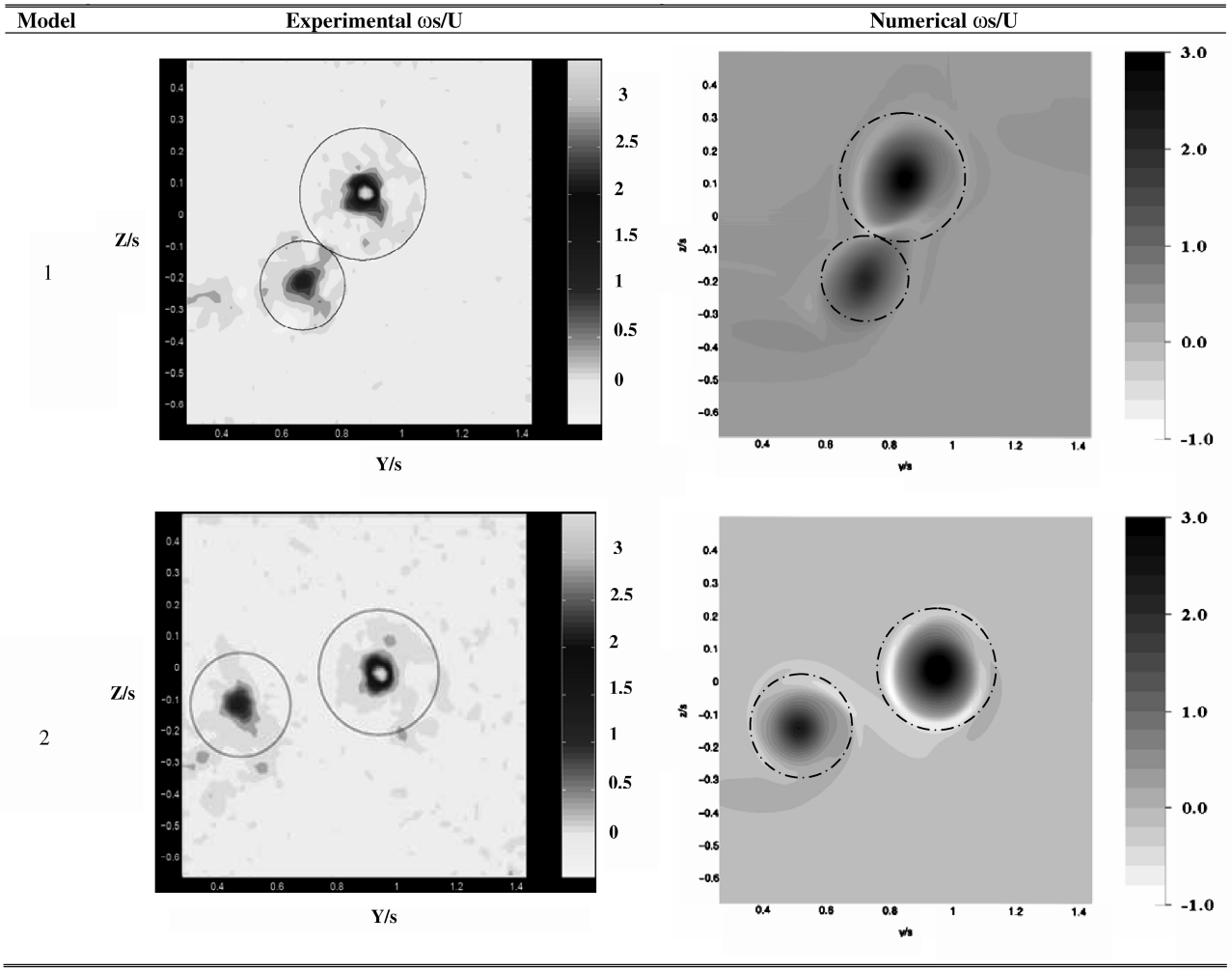

Fig. 7 Vorticity contour levels for models 1 and 2 at 21*c*.

and 3, respectively, which confirms that computational and experimental vorticity data are in good agreement at 4*c*. Vorticity magnitude differences for Models 1 and 2 are also noticed at 21*c*, principally for the flap vortices and the negative vortex region. Computed values at tip and flap core centers, for Models 1 and 2, are increased by 33% and 53%, respectively, compared with experimental data. As explained previously, these vorticity magnitudes correspond to the maximum value of a single cell located exactly at the tip and flap core centers. Surrounding tip vorticity levels at 21*c* for model 1 and model 2 are equal to 3.2 and 3.8, whereas flap vorticity levels are 1.6 and 1.9 for the conventional and the notched wing, respectively. Experimental data do not list any negative area at 21*c* for model 2 whereas computed data do; although the computed values are extremely small. Vorticity values at 80*c* clearly show that tip and flap vortices for model 1 have merged whereas the vortices for model 2 are still distinct. A small region of weak negative vorticity close to the tip vortex is still detected numerically. Ninety percent decays in tip and flap vorticity magnitudes are obtained at 80*c* for the conventional and the notched wings. Decay rates are higher when compared with experimental data. It is expected that if tip and flap vorticity magnitudes for models 1 and 2 could be computed at 132*c*, vorticity values would be slightly lower compared to experimental values shown at 132*c*. Computational dissipation restricts preserving the strength of vortices, particularly at distant regions away from the wings where the grid resolution is lower. Because of some inevitable dissipation and diffusion term errors, the vorticity magnitudes of the vortex cores are not well maintained after significant distances of convection. However, computed vorticity values are still within the range of the experimental values.

Experimental and computed circulation data are now compared at various measurement planes for the conventional and the notched wings (Tables 5 and 6). Numerical data are determined by means of the standard Eqs. (1) and (2). A good similarity can be observed between experimental and computed results for both wing models. The overall total circulation error for the conventional and the notched wings is less than 6% at 4*c*, showing a good agreement between experimental and computed circulation values. Differences in circulation can also be noticed in the negative areas at 4*c* and crossflow planes further downstream. In the contour plots of Figs. 6–8, the negative regions are close to the positive vortices, namely, the tip and the flap vortices. Thus, it is likely that tangential values computed for the negative regions are summed up and averaged with positive values, inducing some errors in computed circulation values. At 21*c*, numerical circulation data differ slightly (error is less than 12%) from experimental data. All numerical circulation values tend to be lower than experimental values, except for the flap circulation values of model 1. A way to explain this variation in circulation results is to suggest that errors found at 4*c* are growing all the way up to 80*c*, resulting in a greater reduction in the accuracy. It is well known that turbulence is created with a wide range of eddy sizes. Thus, to have some extremely accurate set of data, small eddies need to be fully resolved. Unfortunately this is not the case for the Reynolds-averaging method, which models all turbulent eddies. As a result, dissipation and diffusion terms are prone to some errors. Again, it is probable that if the circulation data for models 1 and 2 could be obtained at 132*c*, the computed circulation values would be slightly lower when compared with experimental values. As explained previously, these errors may be due to the intermediate/coarse grid resolution far downstream.

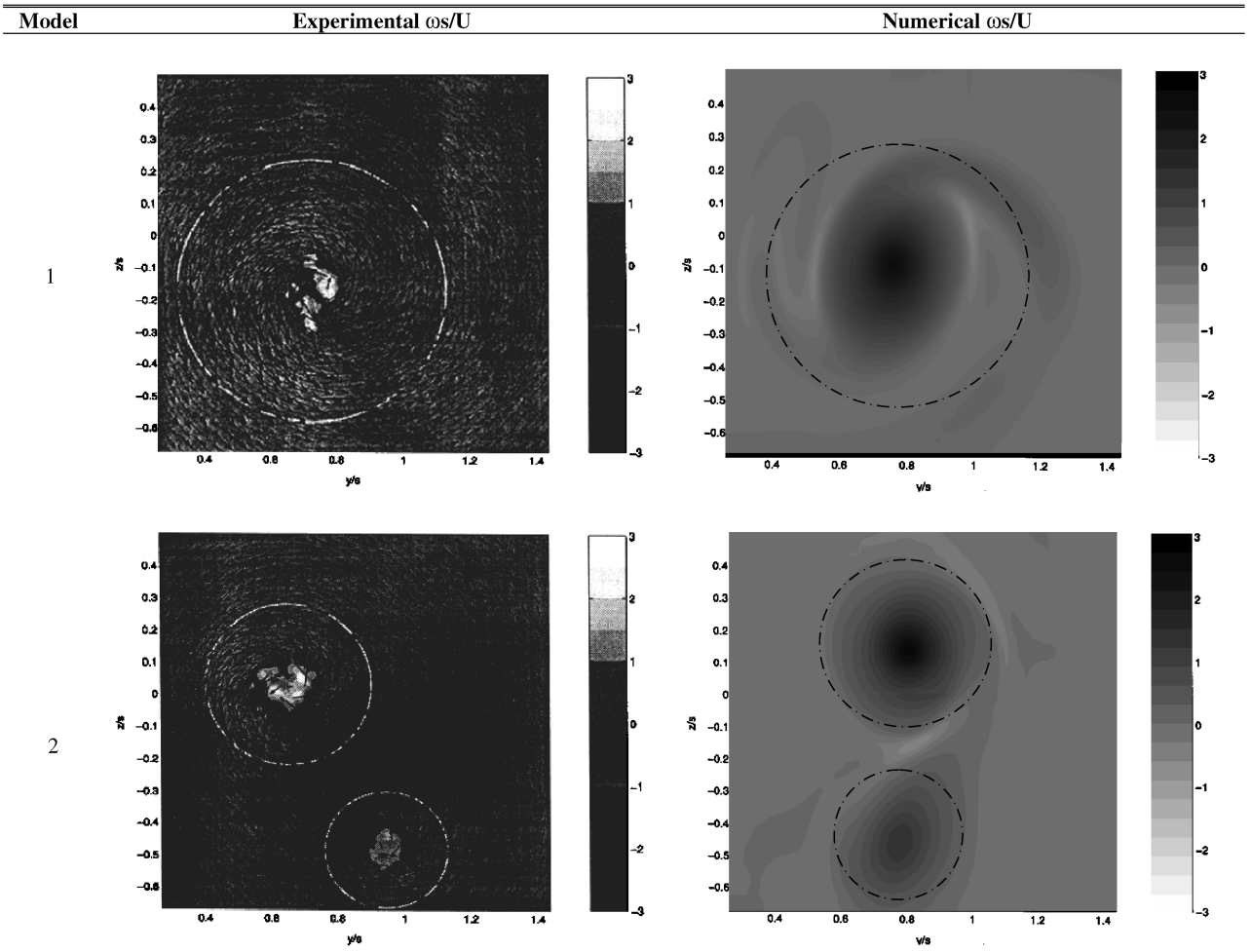

Fig. 8 Experimental vorticity contour levels for models 1 and 2 are given at 132*c* (left-hand side column); computed results are obtained at 80*c* (right-hand side column).

The work presented here has focused on the problem of validating the recent CFD simulations with the available experimental data [9]. Performances of computational models were, therefore, evaluated against the experimental ones. Computational data have demonstrated that the two-equations RNG k–ϵ turbulence model, combined with an appropriate treatment of the near-wall region, is capable of predicting accurately turbulent flow and simulate wake vortices past specifics wing design: in this case, the conventional and the notched geometries. The applied turbulence model predicts similar vortex core contours and locations, even though slight discrepancies occur in vorticity magnitudes and circulation values. Finally, the agreement with experiment remains good, and the discrepancies between experimental and computation solutions are small. Confidence was finally established on the accuracy of the employed CFD method. The second part of this paper considers numerous geometries associated with the notch design. It will be demonstrated that such geometrical combinations considerably modify the wake hazard associated with the present vortex system.

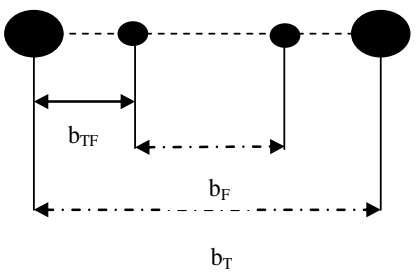

Fig. 9 Vortex spacing (b_T = tip–tip, b_F = flap–flap, b_{TF} = tip–flap).

IV. Results and Discussion: Set 2

A. Wing Models

Having established confidence on the simulation's approach and post-analysis data used, further modeling and computations were attempted. Using previous cross section and shapes as a starting point, a number of geometrical changes for rectangular-notched wings were generated and analyzed computationally. Set 2 includes seven wing models, all associated with the original notch design: models 3 and 4 are presented in set 2a whereas models 5–9 are presented in set 2b. The notch design was kept as original and only the end-tip geometries were varied. Alterations in cut cross section were achieved with respect to distance along the chord (7, 50, and

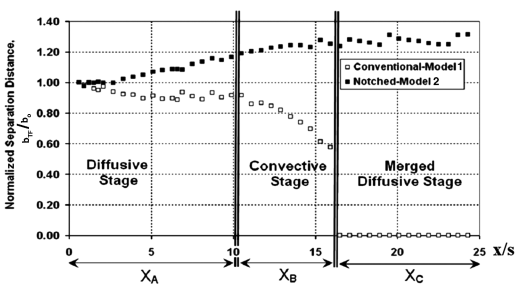

Fig. 10 Evolution of the tip–flap vortex spacing for models 1 and 2.

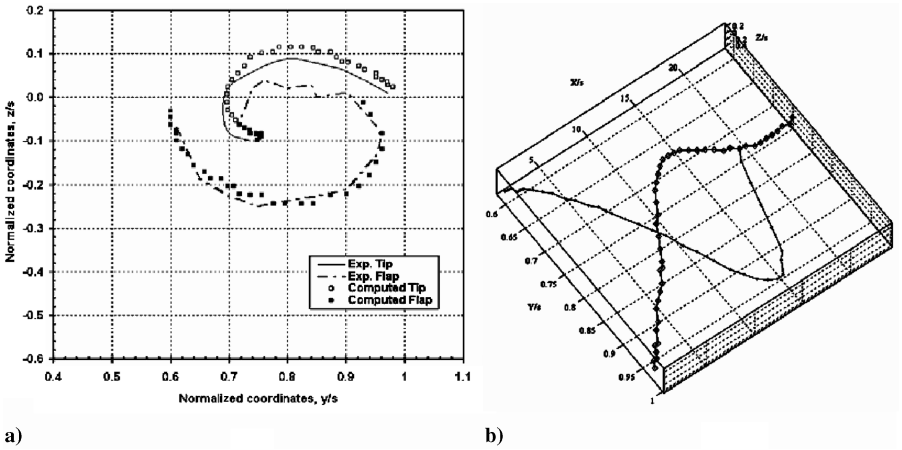

Fig. 11 a) Experimental ($x/c = 132$) and computed ($x/c = 80$) tip and flap vortex trajectories for model 1; b) computed 3-D trajectories: diamonds–tip vortex core, squares–flap vortex core.

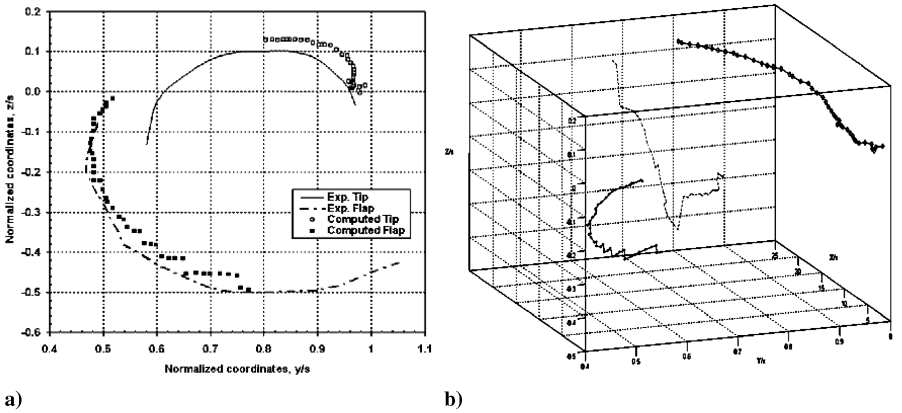

Fig. 12 a) Experimental ($x/c = 132$) and computed ($x/c = 80$) tip and flap vortex trajectories for model 2; b) computed 3-D trajectories: diamonds–tip vortex core, squares–flap vortex core, dotted line–negative patch vortex.

60%) and along the span (75, 80, and 87%). End-tip geometries included triangular and ogee sections. Figures 2 and 3 show a selection of wing models analyzed in this section. The influence of triangular/ogee end-tip geometries on the topology of the wake of a rectangular-notched wing is now investigated.

B. Baseline Analysis

The testing of end-tip shape combinations alone was conducted first in this research work, although detailed vortex dataflow are not presented here. Simulations were performed with triangular and ogee end-tips. The wings did not include the notch design. Results demonstrated that modifying the end-tip shapes greatly influenced the formation, evolution, and merging process of the vortex systems. Significant reductions in tip vortex strength were observed between the conventional wing and the triangular/ogee wings. At all measurement planes the conventional tip vortex was stronger than the triangular/ogee tip vortices. At $1c$, reductions in vorticity magnitude of 57.6 and 41.6% were observed for triangular and ogee tips, respectively, falling to 10.1 and 13.8% at $40c$. At $80c$, the ogee tip produced the greatest decrease in tip vortex strength. Tangential velocities were reduced below those produced by the conventional end-tip by a factor of 5 for a triangular tip and by a factor of 2 for an ogee tip, at $1c$. Further downstream, decreases in tangential velocities for triangular and ogee end-tips were still noticed but by a smaller factor as the cores developed. Circulation data were examined as well, clearly illustrating the dramatic effects of end-tip geometries on tip vortex strength. Circulation values for triangular and ogee shapes, at $40c$ and $80c$ were lowered by 25, 42% and 23, 32%, respectively, compared to the conventional end-tip. Although it was desirable to keep the tip and flap vortices separated, it appeared that the merging process (tip-flap vortex) of the triangular and ogee planform wings was accelerated: an isolated and single vortex was formed for model 1 at precisely $54c$, whereas triangular and ogee vortex systems merged at $36c$ and $38c$, respectively. This clearly indicated that the triangular and ogee configurations generated large and diffusive vortex systems at tip locations. Tip vortices were, therefore, close enough to the flap vortices to destabilize the overall vortex system, accelerating the merging process. Although the tip and flap vortices of the triangular-ogee wings merged, the overall

Table 1 Normalized centroid locations for model 1

	Experimental data		Numerical data	
Plan	y/s	z/s	y/s	z/s
$4c$	0.771	−0.040	0.774	−0.041
$21c$	0.784	−0.079	0.788	−0.076
$80c$	——	——	0.785	−0.098
$132c$	0.769	−0.178	——	——

Table 2 Normalized centroid locations for model 2

	Experimental data		Numerical data	
Plan	y/s	z/s	y/s	z/s
$4c$	0.772	−0.063	0.769	−0.066
$21c$	0.734	−0.072	0.741	−0.069
$80c$	——	——	0.771	−0.139
$132c$	0.760	−0.150	——	——

Table 3 Center core vorticity magnitudes $\omega s/U$ for model 1

Plan	Experimental data			Numerical data		
	Tip	Flap	Neg. Area	Tip	Flap	Neg. Area
$4c$	~3	~3	N/E	12.01	8.100	N/E
$21c$	~3	~1.3	N/E	3.607	2.343	N/E
$80c$	——	——	——	1.433	N/E	N/E
$132c$	~1–2.5	N/E	N/E	——	——	——

Table 4 Center core vorticity magnitudes $\omega s/U$ for model 2

Plan	Experimental data			Numerical data		
	Tip	Flap	Neg. Area	Tip	Flap	Neg. Area
$4c$	~3	~3	~ -3	14.55	7.880	−2.949
$21c$	~3	~1.3	N/E	4.483	2.764	−0.326
$80c$	——	——	——	1.511	0.758	−0.309
$132c$	~1–2.5	~1–2	N/E	——	——	——

strength of their single vortex was reduced when compared with the conventional vortex system. Finally, end-tip shape modifications proved to efficiently reduce wake strengths.

C. Vortex Contours and Spacing b_{TF}

Based on encouraging results presented in the preceding section and because the notch design and the triangular/ogee end-tips have individually positive effects on vortex flow and are, therefore, the key modeling parameter, it was decided to investigate and quantitatively evaluate the combining effects of the notch design and end-tip geometries on wake vortex alleviation. Vortex data for each of the seven models were measured at various locations ranging from $1c$ to $80c$ downstream the trailing edge. Results were then compared with reference models 1 and 2 to determine geometries' influences on core center locations, separation distances, vortex strengths, tangential velocities, and core radii.

Vortex centroid locations are sufficiently varied in all shapes surveyed to draw serious attention to provide a quantitative discussion. Figure 13 depicts center core positions and vorticity contours for models 3, 4, and 6. Major differences are noticed at measurement planes close to the trailing edge. The number of vortices and circulation sign (positive or negative) vary between wing designs. It was found that the original notch wing (model 2) creates three vortices, two positive and one negative (Figs. 6–8). In comparison, model 3–N7Tri75 creates four vortices, two positive and two negative (Fig. 13). Similar contours are also observed for model 4–N7Sik75 and model 6–N50Sik75 (Fig. 13). These new vortices which are either (positive or negative) corotating or counterrotating, depending on the wing shape, are located at the extreme tip top corner. These vortices tend to diffuse extremely quickly and their effects on the diffusive merging process are not known yet. Figure 14 illustrates a sequence of vorticity plots for models 4–N7Sik75, 5–N50Tri75, and 6–N50Sik75 at various crossflow planes. Clearly the vortex spacing, b_{TF}, is greatly influenced by combinations of the notched and the end-tip shape modifications; a fact that is consistently observed in all computed geometries reported herein (Table 7 and Fig. 15). Both triangular and ogee cut sections located at 7% of the chord (models 3 and 4, set 2a) show the merging of their two main vortex systems, namely, the tip and the flap vortex. Merging takes place at $52c$ and $74c$ for models 4–N7Sik75 and model 3–N7Tri75, respectively, compared with $54c$ for the conventional model. Tip vortices produced by wing models 3 and 4 are relatively diffusive. Finally, although the notch design is included in wing models 3 and 4, the tip and flap vortices of the notched-triangular/ogee wings merge. Table 7 and Fig. 15 show that reasonably high vortex separation values are obtained for wing shapes contained in set 2b. Results indicate that the tip and flap vortices for section located at 50 and 60% of the chord do not merge. The triangular shape, located at 50% of the chord and 75% of the span (model 5), produces the highest separation distance between the tip and the flap vortices, whereas model 6–N50Sik75 is seen to produce the lowest vortex separation. Changes in spanwise location clearly introduce higher values of spacing b_{TF} and delay the merging time: vortex separations are equal to 0.954, 1.192, and 1.288 at 75, 80, and 87%, respectively. Table 7 indicates that by moving the ogee end-tip section from 50 to 60% along the chord it slightly increases the separation distance. Yet, vortex separation values obtained for models 8–N50Sik87 and 9–N60Sik87 are still lower than model 5–N50Tri75. Thus, varying the location along the chord and the span does not produce linear variation in vortex separation. Finally, model 5–N50Tri75 produces the largest vortex separation.

D. Vorticity Fields and Circulation

Table 8 and Fig. 16 present the computed vorticity magnitudes as a function of locations downstream the trailing edge of notch-triangular/ogee wings. Note that a nonexistent (N/E) value in vorticity magnitude in Table 8 indicates the merging of the tip vortex with the flap vortex. It can immediately be observed that the magnitude of the tip vortex shed into the flow by the original notched design (model 2) is higher compared to all other geometries, at all surveyed planes. Vorticity magnitudes for models included in set 2 are decreased by values ranging from 50 to 5% at $x/c = 1$ and by 36 to 19% at $80c$, in comparison with model 2. As noticed earlier, results show that even with the notch configuration incorporated in all

Table 5 Circulation values Γ/Us for model 1

Plan	Experimental data				Numerical data			
	Tip	Flap	Neg. Area	Total	Tip	Flap	Neg. Area	Total
$4c$	0.0590	0.0380	N/E	0.1070	0.0569	0.0430	N/E	0.0972
$21c$	0.0580	0.0365	N/E	0.1060	0.0561	0.0414	N/E	0.0926
$80c$	——	——	——	——	0.0811	N/E	N/E	0.0812
$132c$	0.093	N/E	N/E	0.099	——	——	——	——

Table 6 Circulation values Γ/Us for model 2

Plan	Experimental data				Numerical data			
	Tip	Flap	Neg. Area	Total	Tip	Flap	Neg. Area	Total
$4c$	0.0740	0.0450	−0.016	0.1100	0.0686	0.0417	−0.0047	0.1080
$21c$	0.0730	0.0435	N/E	0.1070	0.0676	0.0409	−0.0010	0.0938
$80c$	——	——	——	——	0.0597	0.0306	−0.0009	0.0914
$132c$	0.067	0.034	N/E	0.108	——	——	——	——

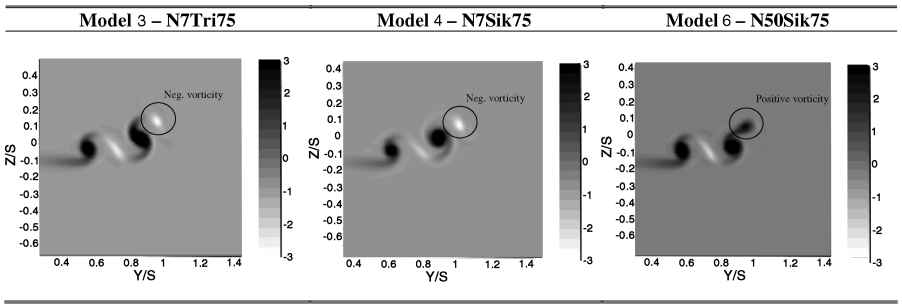

Fig. 13 Vorticity contour levels for models 3, 4, and 6 at 4*c*. New regimes of (positive/negative) vortices are created.

designs, the tip and the flap vortices of some wing designs merge (models 3 and 4). Vorticity values for models 3–N7Tri75 and 4–N7Sik75 are compared with vorticity values of reference model 2 (at 4*c*) and model 1 (at 80*c*). Data show that tip vorticity values are reduced by 31 and 18% for models 3 and 4, respectively, at 4*c*, compared to model 2. At 80*c*, vorticity magnitudes of the merged systems (models 3 and 4) are compared to the vorticity magnitude of the single merged vortex system shed by the conventional wing (model 1). The vorticity values are reduced by 28 and 23% for models 3–N7Tri75 and 4–N7Sik75, respectively. It undoubtedly proves that even though the tip and flap vortices merge for models 3 and 4, the overall strength of their merged vortex is reduced compared to the conventional wing. As compared with all the other models in set 2, model 5–N50Tri75 produces the weakest tip vortex at 4*c* whereas model 6–N50Sik75 produces the least intense tip vortex at 80*c*. Data set depicts that varying the cutting location along the chord and the span creates a clear effect on the vorticity magnitude of the vortex system. Implementing triangular or ogee end-tip sections on notched wings at 7 and 60% of the chord lowers the vorticity magnitude, but not as much as having the sections located at 50% of the chord. End-tip sections located at 60% of the chord clearly tend to reach maximum vorticity values obtained for the original notch wing (model 2). Varying the section locations along the span (towards the tip) clearly increases tip vorticity magnitude as well. Tip vorticity values indicate an increase of 24%, at 1*c*, for the section located at 87% of the span (model 8–N50Sik87) compared with section located at 75% of the span (model 6–N50Sik75). Finally, analyzing data from sections located at 50% of the chord and 75% of the span, between triangular and ogee end-tips, suggest that the ogee shape produces a larger decrease in vorticity magnitude at large distances downstream the tip region. Models 5–N50Tri75 and 6–N50Sik75 are found to be the most effective configurations in reducing vorticity magnitude.

Table 9 indicates that, at data plane 80*c*, tip circulation values for set 2 wing configurations show a marked reduction, compared with original models 1 and 2. Tip vortex circulations produced by new wing shapes (set 2) are lowered by values as high as 68.5%, compared to model 2. It is believed that through the smooth shapes of the triangular/ogee end-tips, discontinuities in local flow are reduced. Model 6–N50Sik75 shows the largest decrease in tip circulation (69%) at 80*c*. However, it is important to bear in mind that low velocities at large distances downstream the tip region introduce a high degree of uncertainty. Tip vortices generated by triangular and ogee tips are very much enlarged and deformed, introducing approximations in integration areas. In fact, the calculation of the circulation at large radii is not fully accurate due to small errors in the velocity measurement being magnified by the large radial distance in the circulation. This is why the authors decided to compare the tangential velocity distributions, as well as further vortex characteristics to identify the optimum design. Yet, model 6–N50Sik75 is found to be the most effective design in reducing tip circulation values.

E. Tangential Velocity Distributions

To provide further insights into wake behavior, tangential velocity values at tip locations are computed and analyzed for set 2 wing models. Set 2a and set 2b present data according to merged and nonmerged vortex systems, respectively. Data from set 2a are compared with reference models 1 and 2, whereas data from set 2b are compared with reference model 2 only. Sequences of tangential velocities for set 2a and set 2b are shown in Figs. 17 and 18. Analyzing Fig. 17 demonstrates that peak-to-peak tangential velocities for model 2 are higher at all measurement planes, except at 80*c*, as compared to models 3–N7Tri75 and 4–N7Sik75. Reductions of 45.5 and 15.6% are noticed at $X/c = 1$ for models 3 and 4, respectively. Note that the tangential peak-to-peak magnitude for model 4 at 80*c* is higher than the original notched design (model 2). Yet, the tangential magnitude of the merged vortex produced by model 4 is less than the conventional model (model 1). Models 3 and 4 (set 2a) clearly show significant improvements in tangential peak-to-peak velocity compared to reference models 1 and 2. The triangular design (model 3) produces a larger reduction in tip tangential velocities, as compared to the ogee design (model 4). Computed data obtained with set 2b wing models present even higher reductions in tangential velocities (Fig. 18). Model 5–N50Tri75 produces the greatest decrease in tangential velocities at first data plane but model 6–N50Sik75 provides the best tangential velocity magnitude reduction at 80*c*. Reductions of peak tangential magnitudes by 65.8 and 43.5% are achieved with models 5–N50Tri75 and 6–N50Sik75, respectively, at 1*c* as compared with model 2. At 21*c*, tangential velocity reduction values are equal to 32.3% for model 5–N50Tri75 and 40.8% for model 6–N50Sik75. Final values at 80*c* are lowered by 26.8 and 35.2% for models 5 and 6, respectively, compared to model 2. Even though data for models 7–N50Sik80 and 9–N60Sik87 are not included within the plots to avoid "cluttering," their respective tangential velocity values lie between the tangential values of models 6–N50Sik75 and 8–N50Sik87, for model 7–N50Sik80, and between the tangential values of models 2 and 8–N50Sik87, for model 9–N60Sik87, clearly demonstrating that varying the chord and the span location affect the tangential velocity distributions. There is an increase in peak tangential magnitude with varying chord (from 50 to 60%) and span locations (from 75 to 87%).

Finally, variation of tangential velocity distributions with far-field distance indicates that set 2a and set 2b wing models have lower peak tangential velocities values than reference models 1 and 2 at all measurement planes. Furthermore, the triangular and ogee end-tip designs (models 5 and 6) located at 50% of the chord and 75% of the span are shown to be the best design in reducing tangential velocity magnitudes.

F. Tip Core Radii Analysis

As evidenced earlier, wing shapes considered in set 2 proved to be of great interest in wake vortex alleviation. Extra vortex characterizing parameters are considered in this section to help in selecting the optimum notched-triangular/ogee wing design. Data presented in this section are divided into two distinct groups representing the tip core growth rate, r_c/r_{co} (Fig. 19) and the size of tip core, r_c/b_o (Fig. 20). A correlation between the core radius growth rate and the end-tip geometries can clearly be established. Figure 19a (set 2a) shows that the tip core growth rates of models 3–N7Tri75 and 4–N7Sik75 are clearly lower than those of reference models 1 and 2, at all measurement planes. This behavior can be explained by the fact that tip core radii generated by set 2a wing

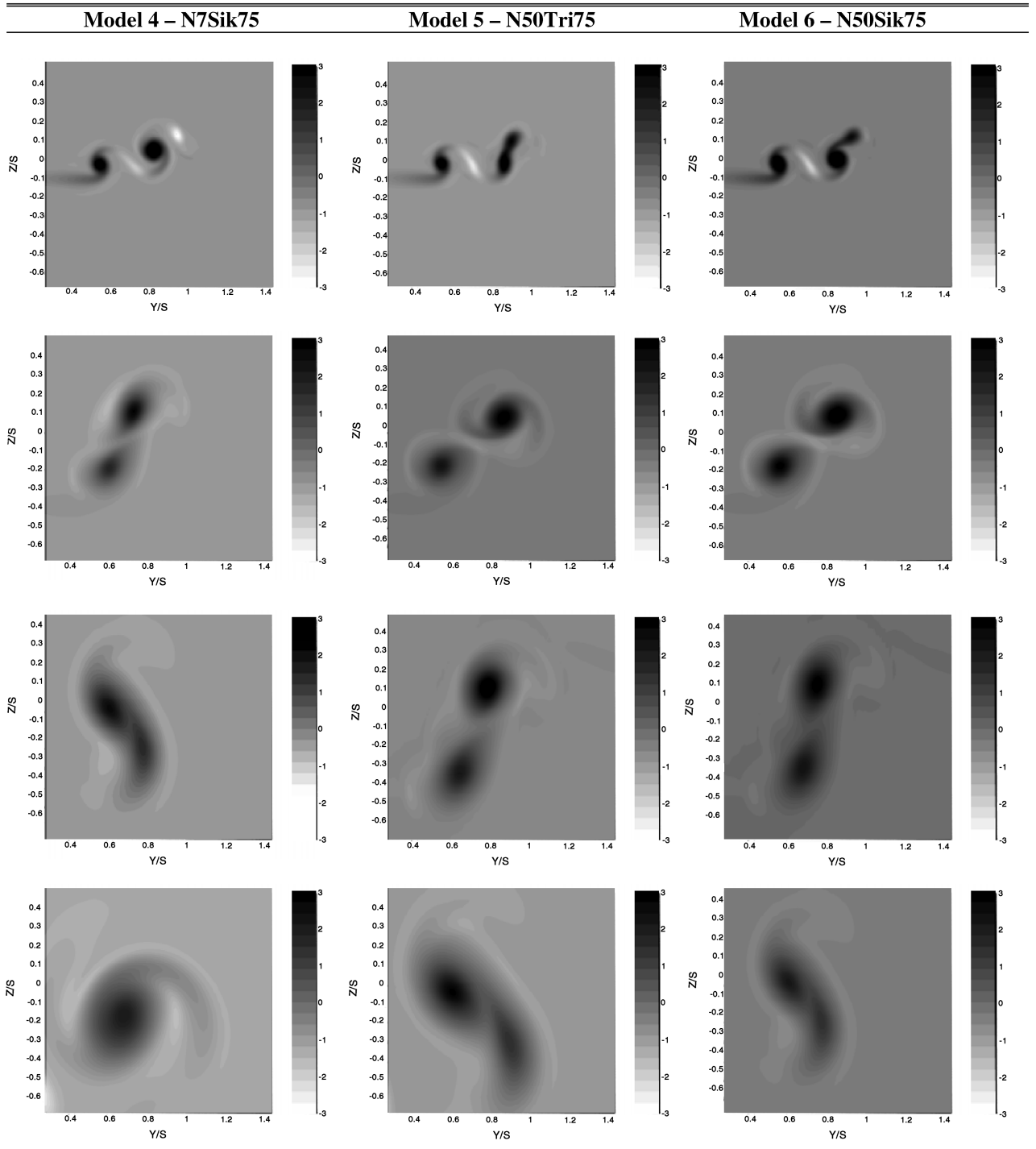

Fig. 14 Vorticity contour levels for models 4, 5, and 6 at 4*c* (first row), 21*c*, 40*c*, and 80*c* (fourth row).

models are originally very large and diffusive and tend to reduce the expansion rate of tip core radii later on. The size of the tip cores for models 3–N7Tri75 and 4–N7Sik75 (set 2a), at first measurement plane, is 65% larger than the tip core size generated by the conventional and the notched wings (models 1 and 2). As it can be observed, the curve for reference model 1 presents a large peak magnitude at location $x/s = 18.3$ (Fig. 19a). It is believed that this is related to the vortex merging process. At this specific location, the tip core is extremely close to the flap core, introducing contours for the tip core which are not well defined and some errors in radii calculations. Similar results are observed for set 2b wing models (Fig. 19b). Tip core expansion rate for model 2 is clearly higher (by 6% at $1c$, and 70% at $80c$) than the tip core expansion rates produced by set 2b wing models, at all surveyed planes. Models having their end-tip sections located at 50% of the chord and at 75% of the span (models 5–N50Tri75 and 6–N50Sik75) are showing the lowest core growth expansion rate. Figure 19b also reveals that tip core growth rate and end-tip sections locations are clearly linked. Varying the end-tip shape location, from 75 to 87% in the spanwise direction, leads to an increment of 64% in tip core size growth rate, at $80c$. Similar results are observed when changes in chord location (from 50 to 60%) are made. An increment of 10% is reached in tip core growth rate at $80c$. No significant variations in tip core growth rate are observed between model 5–N50Tri75 and model 6–N50Sik75.

Significant increases in tip core size, relative to initial spacing b_o are observed for set 2a and set 2b (Fig. 20), clearly indicating that all

Table 7 Dimensionless spacing values b_{TF}/b_o

Plan	Numerical data								
	M-1 Reference	M-2 Reference	M-3 N7Tri75	M-4 N7Sik75	M-5 N50Tri75	M-6 N50Sik75	M-7 N50Sik80	M-8 N50Sik87	M-9 N60Sik87
80c	0	1.314	0	0	1.355	0.954	1.192	1.288	1.299

Table 8 Numerical center core vorticity magnitude $\omega s/U$

Model	Tip vortex				Flap vortex				Neg. Area			
	4c	21c	40c	80c	4c	21c	40c	80c	4c	21c	40c	80c
2–Reference	14.55	4.48	2.78	1.51	7.88	2.76	1.52	0.75	−2.94	−0.32	−0.32	−0.31
3–N7Tri75	10.12	3.64	1.93	1.04	7.87	2.34	1.32	N/E	−1.75	−0.38	N/E	N/E
4–N7Sik75	11.89	3.31	1.71	1.11	7.92	2.38	1.25	N/E	−1.42	−0.51	−0.20	N/E
5–N50Tri75	7.01	3.20	2.16	1.11	7.81	2.34	1.32	0.69	−2.25	−0.37	N/E	N/E
6–N50Sik75	9.65	3.02	1.85	0.97	7.84	2.32	1.35	0.73	−1.89	−0.32	N/E	N/E
7–N50Sik80	11.12	3.56	2.08	1.04	7.83	2.32	1.36	0.65	−2.10	−0.35	N/E	N/E
8–N50Sik87	12.74	3.71	2.15	1.05	7.74	2.33	1.34	0.61	−2.86	−0.44	N/E	N/E
9–N60Sik87	13.02	3.89	2.48	1.24	7.78	2.39	1.46	0.62	−2.88	−0.41	N/E	N/E

end-tip modifications involved in set 2 are more diffusive and produce larger tip cores (increased by an average factor of 3) than reference models 1 and 2. Like model 1, model 4–N7Sik75 presents a peak at $x/s = 18.3$ which is once again attributed to the merging process (Fig. 20a). It is also believed that if data were available at further measurement planes, model 3–N7Tri75 would also presents such a raise in tip core size: the merging of the tip and flap vortices of model 3–N7Tri75 being evaluated at 74c downstream the trailing edge. Increases in tip core size for set 2b wing models are presented in Fig. 20b. Model 6–N50Sik75 presents the highest tip core radius at 1c, over all end-tip shape modifications involved in set #2. Varying the span position from 75% to 87 % (models VI-N50Sik75 and VIII-N50Sik87) decreases the tip core radius by an average value of 42%. Similar results in tip core size are observed when changes in chord location from 50 to 60% are made (models 8–N50Sik87 and 9–N60Sik87). Reductions in tip core radii vary from 25% at $x/c = 1$, to 9% at 80c. Finally, tip vortices generated by triangular and ogee end-tip configurations are extremely diffusive, generating large vortex cores.

Vortex dynamics for notched-triangular/ogee wings were measured over a wide range of end-tip shapes and downstream distances. The following conclusions can be drawn from data set 2: over the entire range of configurations examined, it was found that combining the notched design to triangular/ogee end-tip shapes produced a decrease in vortex spacing when compared with the original notched wing, except for model 5–N50Tri75, which showed the highest vortex separation at 80c. The drop in vortex spacing has been found to be a function of the end-tip location along the chord and along the span. It was noticed that the notched design associated with specific end-tip configurations did not always prevent the merging of the tip and flap vortices. Tip and flap vortices generated by wing models having their end-tip shapes located at 50 and 60% of the chord remained distinct and separated. Further insights were also gained by examining vortex strength data. Set 2 results reveal that significant large reductions in vortex strengths were observed at all measurements planes when triangular/ogee sections were used in place of conventional rectangular end-tip geometries (reference models 1 and 2). Model 5–N50Tri75 has the greatest reduction in tip vorticity and tangential magnitude at 4c, whereas model 6–N50Sik75 has the greatest reduction in circulation values, tip vorticity, and tangential magnitude from 21c to 80c. Tip center core vorticity magnitude for models 5–N50Tri75 and 6–N50Sik75, at 4c and 80c, are lowered by 52 and 36%, respectively, when compared with reference model 2. Furthermore, tip vortices formed by the notched-triangular/ogee wings are extremely diffused at all measurement planes examined. Tip core diameter generated by set 2 wing models are substantially larger than that of the original models 1 and 2. Finally, of all the notched-triangular/ogee wing geometries tested, model 6–N50Sik75 was found to be the best configuration and the most effective wing geometry for wake alleviation.

V. Conclusions

The use of computational fluid dynamics for simulating the formation and development of aircraft trailing vortices has been analyzed. Initially, the applicability of CFD to the simulation of rectangular wings wake vortices was investigated via comparisons with experimental data sets. Results of Sec. III demonstrated the ability of the Reynolds-averaged Navier–Stokes equations to reproduce the global topology of trailing vortex systems as they evolve downstream. Vortex quantities were found to be consistent

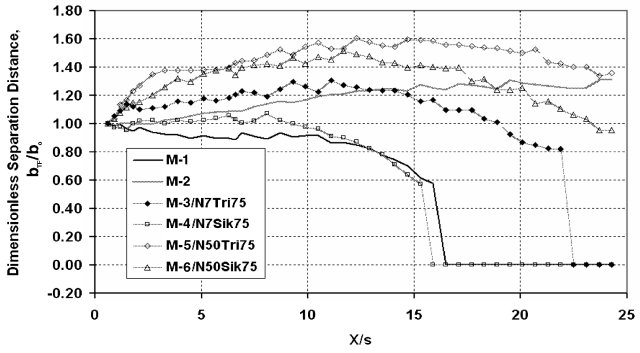

Fig. 15 Evolution of the normalized vortex separation b_{TF} vs convection distance X/s (set 2).

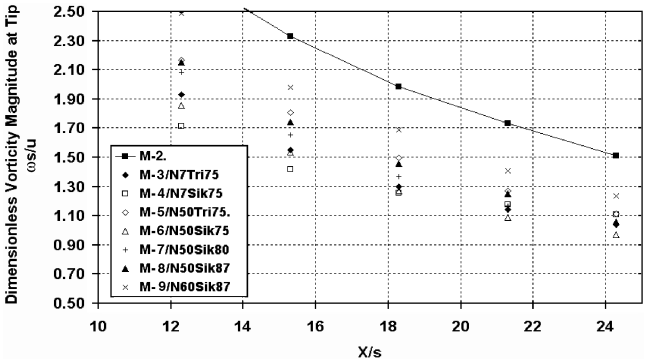

Fig. 16 Tip vortex strengths $\omega s/U$ as a function of vortex age for set 2.

Table 9 Tip circulation values Γ/Us

Plan	Numerical data								
	M-1 Ref.	M-2 Ref.	M-3 N7Tri75	M-4 N7Sik75	M-5 N50Tri75	M-6 N50Sik75	M-7 N50Sik80	M-8 N50Sik87	M-9 N60Sik87
80*c*	0.0811	0.0597	0.0394	0.0579	0.0287	0.0188	0.0279	0.0305	0.0384

with the experimental data. A good correspondence with experiment was achieved up to 80*c*.

The potential to alleviate the wake vortex hazard posed to following aircraft, while keeping the tip and flap vortices distinct, has been demonstrated in Sec. IV. Results show that the notched-triangular/ogee wings generate a trailing vortex wake that has significant wake alleviation properties. Vortex dynamics (vortex strength, vortex shedding, and roll-up process) were significantly modified by varying the end-tip shapes. Ninety degree corners were replaced by smooth triangular and ogee sections. As a result, vorticity magnitude and circulation values were markedly reduced. Data clearly indicated that vortex structures were modified in a favorable way. Extreme diffused core vortices were created, affecting the vortex decay process. In addition, end-tip shape

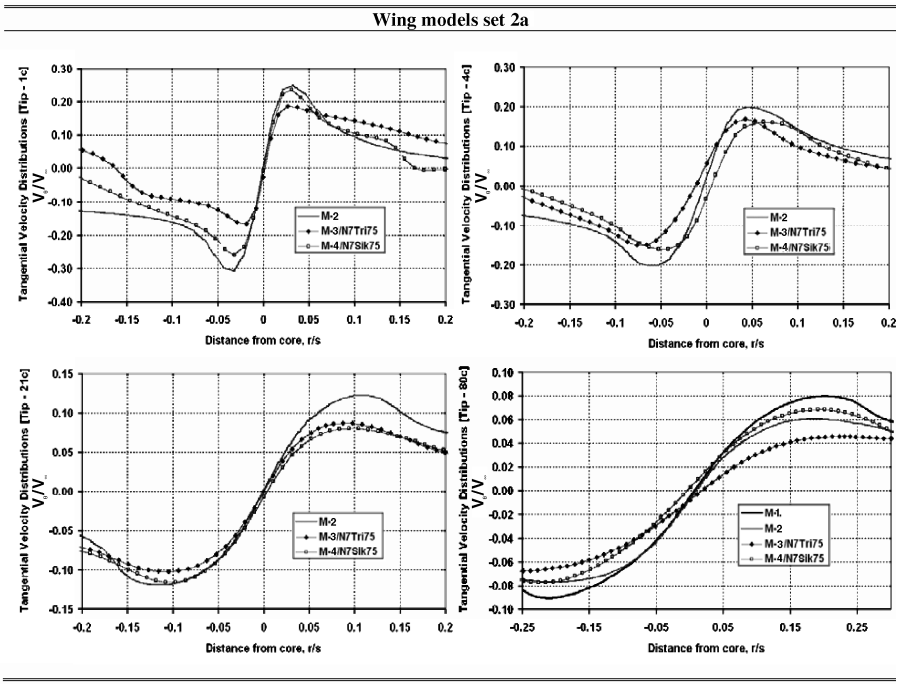

Fig. 17 Sequence of tip tangential velocity distributions for set 2a at 1*c*, 4*c*, 21*c*, and 80*c*.

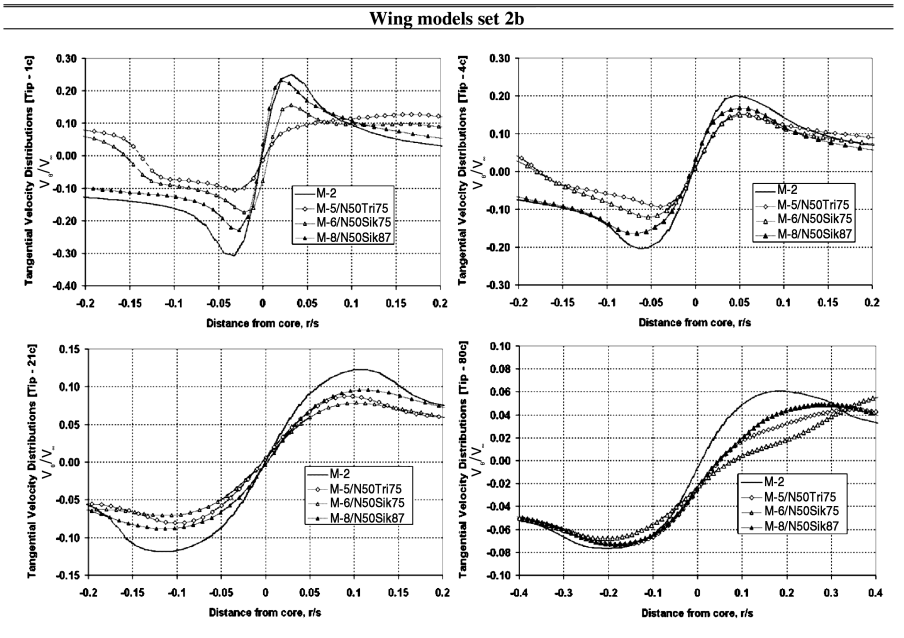

Fig. 18 Sequence of tip tangential velocity distributions for set 2b at 1*c*, 4*c*, 21*c*, and 80*c*.

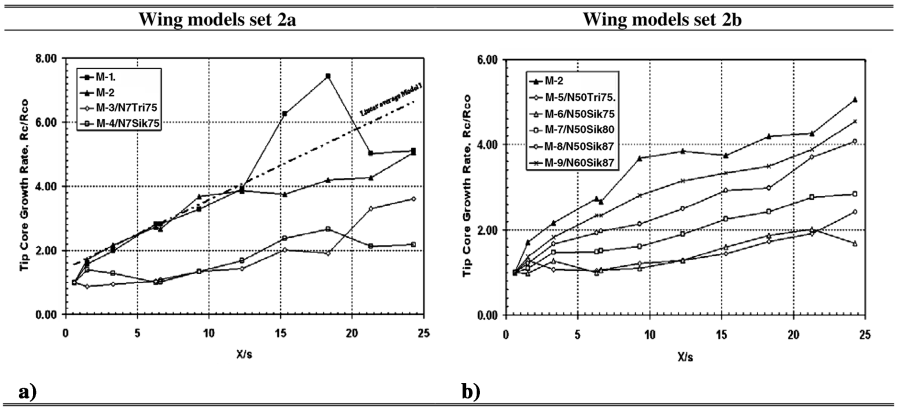

Fig. 19 Tip core expansion rate (relative to the initial core radii r_{co}) for sets 2a and 2b. The dashed line represents the linear average for model 1.

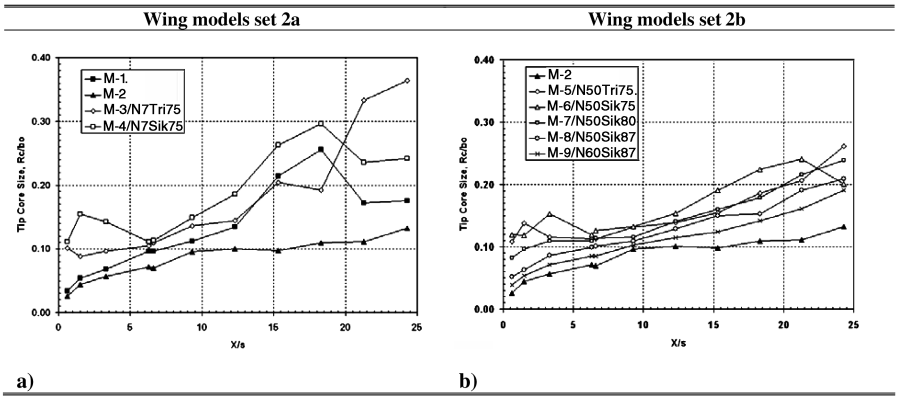

Fig. 20 Tip core expansion rate (relative to the initial spacing b_o) for sets 2a and 2b.

modifications proved to efficiently reduce the high tangential velocities generally found in the tip core vortex of rectangular wings. The strong tip vortex, concentrated in a small area, was therefore no longer present. Finally, results demonstrated that geometrical wing modifications play a capital role in reducing wake vortices produced by rectangular wings. The diffusive properties created in the wake of the notched-ogee wings offer an appropriate mechanism for an effective reduction of the complex wake vortex phenomenon. The present research work could be extended to other applications. For instance, notched-ogee designs could be applied to the outer tips of helicopter blades to reduce the noise and vibrations induced by the blades as they pass through the air.

To conclude, data presented in this paper constitute a promising way forward in the field of wake vortex hazard reduction and it is considered worthy, by the authors, of further analysis. Further computational investigations for swept wings are being currently performed by the authors.

Acknowledgments

The authors would like to acknowledge W. R. Graham and S. W. Park for their active assistance in providing experimental data resources and many fruitful discussions. The authors are grateful to the referees for suggestions on improving the original manuscript.

References

[1] Heitmeyer, R., "Biometric ID and MRTDs Will Help Generate Future Airport Capacity," *International Airport Review*, Vol. 5, No. 1, 2001, pp. 60–63.

[2] Gerz, T., Holzapfel, F., and Darracq, D., "Aircraft Wake Vortices—A Position Paper," *WakeNet—the European Thematic Network on Wake Vortex*, Vol. 6,April 2001, pp. 1–43.

[3] Hunecke, K., "Wake Vortex Control—A Challenge for Large Transport Aircraft," *Air & Space Europe*, Vol. 3, Nos. 3–4, 2001, pp. 209–213.

[4] Chambers, J. R., "Concept to Reality: Contributions of the NASA Langley Research Center to U.S. Civil Aircraft of the 1990s," NASA History Series, NASA SP-2003-4529, Dec. 2002.

[5] Lee, G. H., "Trailing Vortex Wakes," *The Aeronautical Journal*, Vol. 79, No. 271, Sept. 1975, pp. 377–388.

[6] Kirkman, K., Brown, L., Clinton, D., and Goodman, A., "Evaluation of Effectiveness of Various Devices for Attenuation of Trailing Vortices Based on Model Tests in a Large Towing Basin," NASA CR-2202, Dec. 1973.

[7] Rossow, V. J., "Lift-Generated Vortex Wakes of Subsonic Transport Aircraft," *Progress in Aerospace Sciences*, Vol. 35, No. 6, 1999, pp. 507–660.

[8] Graham, W. R., "Optimizing Wing Lift Distribution to Minimize Wake Vortex Hazard," *The Aeronautical Journal*, Vol. 106, No. 1062, Aug. 2002, pp. 413–426.

[9] Graham, W. R., Park, S. W., and Nickels, T. B., "Trailing Vortices from a Wing with a Notched Lift Distribution," *AIAA Journal*, Vol. 41, No. 9, 2003, pp. 1835–1838.

[10] Ortega, J. M., Bristol, R. L., and Savaş, Ö., "Wake Alleviation Properties of Triangular-Flapped Wings," *AIAA Journal*, Vol. 40, No. 4, April 2002, pp. 709–721.

[11] Rorke, J. B., and Moffit, R. C., "Wind Tunnel Simulation of Full Scale Vortices," NASA CR-2180, March 1973, pp. 1–112.

[12] Mantay, W. R., Shidler, P. A., and Campbell, R. L., "Some Results of the Testing of a Full-Scale Ogee-Tip Rotor," *Journal of Aircraft*, Vol. 16, No. 3, March 1979, pp. 215–234.

[13] Davidson, P. A., *Turbulence: An Introduction for Scientists and Engineers*, 1st ed., Oxford Univ. Press, Oxford, 2004, Chap. 4.

[14] FLUENT Ver. 6.2 User's guide, Fluent, Inc., PathScale Corporation, Lebanon, Jan. 2005.

[15] Choudhury, D., "Introduction to the Renormalization Group Method and Turbulence Modelling," Fluent, Inc. Technical Memorandum TM-107, 1993.

[16] Cerretelli, C., and Williamson, C. H. K., "The Physical Mechanism for Merging of Trailing Vortices," *Journal of Fluid Mechanics*, Vol. 475, No. 1, Jan. 2001, pp. 41–77.